Band head spin assignment of superdeformed bands in ^{86}Zr

Anshul Dadwal H. M. Mittal[1)]

Dr. B. R. Ambedkar National Institute of Technology, Jalandhar 144011, India

Abstract: Two parameter expressions for rotational spectra viz. variable moment of inertia (VMI), *ab* formula and three parameter Harris ω^2 expansion are used to assign the band head spins (I_0) of four rotational superdeformed bands in ^{86}Zr. The least-squares fitting method is employed to obtain the band head spins of these four bands in the $A\sim 80$ mass region. Model parameters are extracted by fitting of intraband γ-ray energies, so as to obtain a minimum root-mean-square (rms) deviation between the calculated and the observed transition energies. The calculated transition energies are found to depend sensitively on the assigned spins. Whenever an accurate band head spin is assigned, the calculated transition energies are in agreement with the experimental transition energies. The dynamic moment of inertia is also extracted and its variation with rotational frequency is investigated. Since a better agreement of band head spin with experimental results is found using the VMI model, it is a more powerful tool than the *ab* formula and Harris ω^2 expansion.

Keywords: Superdeformed bands, VMI model, *ab* formula, Harris ω^2 expansion

PACS: 21.10.Hw, 21.60.-n, 27.50.+e. **DOI:** 10.1088/1674-1137/40/11/114103

1 Introduction

The discovery of superdeformed states in nuclei is one of the most remarkable discoveries of the 20$^{\rm th}$ century, since the nuclei are exposed to extreme conditions of deformation and angular momentum in order to obtain superdeformation. The existence of superdeformation was predicted by Strutinsky [1] and later confirmed experimentally by Twin et al. [2] in the ^{152}Dy nucleus. With the development of large γ-ray detectors, new mass regions of superdeformation have been explored. Various superdeformed (SD) bands are currently available in the $A\sim 190, 150, 130$ and 80 mass regions. Usually, SD bands are identified by transitions from equally spaced energy levels, which results in a series of γ-ray spectra. However, the spins of SD bands were not established experimentally until the discovery of γ-rays connecting states of yrast SD bands ^{194}Hg(1) to normal deformed (ND) states [3]. Soon after, the spins and excitation energies of yrast SD band ^{194}Pb(1) [4–6] and ^{194} Hg(3) [7] were established. Besides such exceptions, the estimated spins of other SD bands in different mass regions have uncertainties of $\approx 1-2\hbar$. The level spin determination of superdeformed states is crucial to understand the physics behind them. In the past few years, many approaches have been made to assign the spins of SD bands [8–11]. Microscopic models such as the exponential model [12], cranked shell model [13], cranking Bohr-Mottelson Hamiltonian [14] etc. have also been used to assign reliable spins to SD bands.

Superdeformation spectroscopy has provided us with much information regarding the behaviour of moments of inertia (MOI) in SD nuclei. Two types of MOI characterize nuclei in SD states, viz. kinematic ($\Im^{(1)}$) and dynamic MOI ($\Im^{(2)}$). Since $\Im^{(1)}$ depends upon spin proposition, $\Im^{(2)}$ is frequently studied in SD states. A smooth rise of $\Im^{(2)}$ with increasing rotational frequency ($\hbar\omega$) is observed in the $A\sim 190$ mass region whereas in the $A\sim 150$ mass region, different behaviour of $\Im^{(2)}$ with $\hbar\omega$ is observed. A smooth rise of $\Im^{(2)}$ with $\hbar\omega$ in $A\sim 190$ is interpreted as alignment of both high-N quasiprotons and quasineutrons and reduction in pairing [15, 16]. The projected shell model (PSM) interpreted [17] this smooth rise in MOI as a combination of the Coriolis antipairing effect (CAP) effect and rotation alignment of high-j pairs. An interesting feature of $\Im^{(2)}$ in the $A\sim 190$ mass region is the observation of "flat bands" where $\Im^{(2)}$ does not display a rise with $\hbar\omega$. Pauli blocking [18] of intruder quasiproton and quasineutron is held responsible for the reduced slope of $\Im^{(2)}$. Microscopic models such as PSM also reveal the interesting features of SD bands in the lower mass region. Application of PSM to $A\sim 60$ reveals [19] that alignment of $g_{9/2}$ proton and neutron pairs dominates, which results in low level densities near the Fermi level. Also, anomalies in the MOI of SD bands in ^{132} Ce was illustrated [20] as the intersection of four

Received 22 Aug. 2016

1) E-mail: mittal.hm@lycos.com

bands at a point where the MOI lose intensity rapidly. Experimentally, kinematic and dynamic moments of inertia can be extracted from the observed E_γ transition energies by the difference quotient.

Encouraged by SD band availability in the higher mass region ($A\sim190,150$) and motivated by predictions of cranked Strutinsky calculations, numerous searches have been undertaken to discover SD nuclei in the lower mass region ($A\sim80$). However, these searches were hampered by various experimental difficulties. With the advent of large γ-ray detectors (Eurogam I array), Baktash et al. [21] in 1995 provided the first evidence of high spin superdeformation in the lower mass region with particle numbers $N,Z\approx40$. Large deformations in this mass region are stabilized through a decrease in surface energy and more rapid decrease in Coulomb energy. In general, most of the nuclei are axially symmetric in shape, but the discovery of triaxial superdeformed bands in ^{163,165,167}Lu [22–24] and ^{171}Ta [25] opens a new regime of SD bands where collective rotations are possible about all the three axes involving three unequal moment of inertia ($\Im_x>\Im_y\neq\Im_z$). A triaxial SD band $A\sim80$ mass region was found by Sarantites et al. [26]. They observed a total of four bands in ^{86}Zr, out of which three (^{86}Zr(1), ^{86}Zr(2) and ^{86}Zr(4)) were found to be triaxial SD bands. Through the decay of ^{86}Zr(1) to ND states they estimated spin $I_0=21.7\pm1.5\hbar$. However, reliable spins of other SD bands were not possible using the same method.

Currently, many theoretical methods, like Bohr-Mottelson's $I(I+1)$ expansion [27], Harris ω^2 expansion [28, 29], the ab formula [30–33], variable moment of inertia (VMI) [34], variation of moments of inertia with angular momentum [35] etc., are available to provide a reliable way for spin assignment. In this paper, we have evaluated the spins of all four bands of ^{86}Zr using the VMI model, ab formula and Harris ω^2 expansion.

2 Rotational energy formulae

2.1 Variable moment of inertia model

Mariscotti et al. [34] proposed the VMI model, which gives energy level with angular momentum (I) as the sum of the potential energy term $\propto(\Im_I-\Im_0)^2$ (where $\Im_0$ represents the ground state moment of inertia (MoI)) and the rotational energy term $\hbar^2(I(I+1))/2\Im_I$. The two parameter VMI model defines each nucleus by band head moment of inertia ($\Im_0$) and restoring force constant (C). The energy of a level with spin (I) is given by (taking $\hbar=1$)

$$E_I=E_0+\frac{I(I+1)}{2\Im_I}+\frac{C(\Im_I-\Im_0)^2}{2}. \tag{1}$$

The moment of inertia ($\Im_I$) of the nucleus is calculated from the equilibrium condition

$$\frac{\partial E(\Im_I)}{\partial\Im_I}, \tag{2}$$

which yields

$$\Im_I^3-\Im_I^2\Im_0-\frac{I(I+1)}{2C}=0. \tag{3}$$

This cubic equation has one real root for any positive value of $\Im_0$ and C. From Eq. (1) and Eq. (3) we get

$$E_I=E_0+\left[\frac{I(I+1)}{2\Im_0}\right]\left[1+\frac{I(I+1)}{4C(\Im_0)^3}\right]. \tag{4}$$

Since intraband energies and intensities are the only spectroscopic properties whose information are available for superdeformed bands, one may choose to fit E_γ transitions as:

$$E_\gamma=E(I)-E(I-2). \tag{5}$$

Using Eq. (4) and Eq. (5) the transition energy for superdeformed bands is expressed as

$$E_\gamma(I\longrightarrow I-2)=\frac{[I(I+1)-(I-2)(I-1)]}{2\Im_0}+\frac{[I(I+1)]^2-[(I-2)(I-1)]^2}{8C(\Im_0)^4}. \tag{6}$$

The parameters $\Im_0$ and C can be obtained by fitting the E_γ transitions for the superdeformed cascade. The quantity σ, which provides the softness of the nucleus, can be derived using Eq. (3) as follows:

$$\frac{1}{\Im_I}\frac{\mathrm{d}\Im_I}{\mathrm{d}I}=[(2I+1)/2C(\Im_I)^2(3\Im_I-2\Im_0)]. \tag{7}$$

For the particular case of $I=0$, we get

$$\sigma=\left[\frac{1}{\Im_I}\frac{\mathrm{d}\Im_I}{\mathrm{d}I}\right]_{I=0}=\frac{1}{2C(\Im_0)^3}. \tag{8}$$

2.2 The ab formula

From experimental level systematics and alternatively from nuclear hydrodynamics, Holmberg and Lipas [30] derived the two parameter ab formula

$$E(I)=a\left\{\sqrt{1+bI(I+1)}-1\right\}, \tag{9}$$

where a and b are the fitting parameters.

The same expression was derived by Wu et al. [31, 32] using the Bohr Hamiltonian. Using Eq. (5) and Eq. (9), we get

$$E_\gamma(I)\equiv E_\gamma(I\longrightarrow I-2)=a\left[\sqrt{1+bI(I+1)}-\sqrt{1+b(I-2)(I-1)}\right]. \tag{10}$$

The parameters a and b are obtained by least-squares fitting of observed transition energies. Using parameters a and b, the kinematic and dynamic moments of inertia are extracted from them as follows

$$\Im^{(1)} = \Im_0 \left[1 - \frac{(\hbar\omega)^2}{a^2 b}\right]^{-1/2}, \tag{11}$$

$$\Im^{(2)} = \Im_0 \left[1 - \frac{(\hbar\omega)^2}{a^2 b}\right]^{-3/2}, \tag{12}$$

where $\Im_0 = \dfrac{\hbar^2}{ab}$ is the band head moment of inertia. Rotational frequency ($\hbar\omega$) is defined as

$$\omega = \frac{1}{\hbar}\frac{\mathrm{d}E}{\mathrm{d}I_x} \approx \frac{1}{\hbar}\frac{\mathrm{d}E}{\mathrm{d}I}.$$

Since $\hbar\omega$ is not the directly observed quantity, it is estimated [36] from the observed E_2 transition energies by the difference quotient

$$\hbar\omega(I) = [E_\gamma(I) + E_\gamma(I+2)]/4000. \tag{13}$$

2.3 Harris ω^2 expansion

Harris [28, 29] showed that the nuclear rotation energy can be expanded in an even power series of rotational frequency rather than $I(I+1)$ as follows,

$$E(\omega) = \alpha\omega^2 + \beta\omega^4 + \gamma\omega^6 + \delta\omega^8 + ... \tag{14}$$

Here only three parameters are taken. Hence we can write

$$E(\omega) = \alpha\omega^2 + \beta\omega^4 + \gamma\omega^6. \tag{15}$$

Using the relation between energy E and spin I

$$\frac{\mathrm{d}E}{\mathrm{d}\omega} = \frac{\mathrm{d}E}{\mathrm{d}I}\frac{\mathrm{d}I}{\mathrm{d}\omega} = \hbar\omega\Im^{(2)}, \tag{16}$$

$\Im^{(2)}$ takes the form

$$\Im^{(2)} = 2\alpha + 4\beta\omega^2 + 6\gamma\omega^4 (\hbar^2 \mathrm{MeV}^{-1}). \tag{17}$$

This can be rewritten as

$$\Im^{(2)} = A + B\omega^2 + C\omega^4, \tag{18}$$

since $\Im^{(2)} \approx \hbar\dfrac{\mathrm{d}I}{\mathrm{d}\omega}$. Spin can be obtained by integrating $\Im^{(2)}$ with respect to ω and we get

$$I = A\omega + (B/3)\omega^3 + (C/5)\omega^5 + i_0, \tag{19}$$

where i_0 is the constant of integration and known as aligned angular momentum. In the $A \sim 190$ mass region, for odd-A, nuclei i_0 can take either 0 or $\dfrac{1}{2}$ value.

The dynamic moment of inertia can be estimated from the following relations [36]:

$$\Im^{(2)}(I) = 4000/[E_\gamma(I+2) - E_\gamma(I)], \tag{20}$$

where $E_\gamma(I)$ is the energy difference between the $(I+2)^{\mathrm{th}}$ and $(I)^{\mathrm{th}}$ level. The uncertainty for the last significant digit in $\Im^{(2)}$ is calculated as

$$\left[\sqrt{(\Delta E_\gamma(I+2))^2 + (\Delta E_\gamma(I))^2}/E_\gamma(I+2) - E_\gamma(I)\right] \times \Im^{(2)}(I),$$

where $\Delta E_\gamma(I)$ is the uncertainty in intraband γ-transitions.

3 Results and discussion

Intraband γ-transition energy is the only spectroscopic information available about SD bands which is universally available. SD rotational bands are recognized by the cascade

$$I_0 + 2n \to I_0 + 2n - 2 \to, \cdots, \to I_0 + 4 \to I_0 + 2 \to I_0,$$

and transition energies $E_\gamma(I_0 + 2n)$, $E_\gamma(I_0 + 2n - 2), \cdots$, $E_\gamma(I_0 + 4)$ and $E_\gamma(I_0 + 2)$ from these equally spaced levels. These transition energies are least-squares fitted in Eqs. (6), (10) and (18) with fitting parameters $\Im_0, C$, a, b and A, B, C respectively. In this approach, a comparison between calculated transition energies and experimental transition energies is made. It was found that the root-mean-square (rms) deviation (χ) of calculated values with experimental values depends upon the prescribed level spins. Whenever an accurate band head spin (I_0) is assigned, the calculated transition energies agree well with observed transition energies. But, if I_0 is artificially shifted from the correct spin value even by ± 1, the rms deviation increases immensely. We have

$$\chi = \left[\frac{1}{n}\sum_{n=1}^{n}\left(\frac{E_\gamma^{\mathrm{cal}}(I_i) - E_\gamma^{\mathrm{exp}}(I_i)}{E_\gamma^{\mathrm{exp}}(I_i)}\right)^2\right]^{1/2}, \tag{21}$$

where n is the number of transitions involved in the fitting.

E_γ transition energies of the ^{86}Zr band indexed in the table of superdeformed bands [37] and continuously updated ENSDF database [38] have been fitted to the VMI model, ab formula and Harris ω^2 expansion. The values of different fitting parameters are obtained. The values of band head spins obtained from the rotational energy formulae are listed and a comparison with other experimental data made in Table 1.

Table 1. Band head spin (I_0) obtained from various models/formulae of ^{86}Zr. Here 1, 2, 3 and 4 in parenthesis represent band 1, band 2, band 3, and band 4 respectively. The E_γ value marked by an asterisk (*) represents a tentative transition.

SD band	$E_\gamma(I_0+2\rightarrow I_0)$/keV	VMI model	*ab* formula	Harris ω^2 expansion	Ref. [26]
^{86}Zr(1)	1518	24	19	25	23
^{86}Zr(2)	1577	22	13	43	22
^{86}Zr(3)	1866*	24	32	20	25
^{86}Zr(4)	1648	23	14	38	23

Band head spins obtained from the *ab* formula deviate greatly from the values given experimentally [26] for the obvious reason that this formula is valid only for nuclei with small axial asymmetry [31, 32] ($\sin^2 3\gamma \ll 1$). It is also worth mentioning that the *ab* formula is valid for the low spin region before backbending. Spins calculated from Harris ω^2 expansion also have a large deviation, but the band head spin obtained from the VMI model is in agreement with experimental results. Band head spins of all four bands in ^{86}Zr obtained from χ plots using the VMI model are shown in Fig. 1. Since rms deviation depends upon the number of transitions involved, we have ignored highest transition (E_γ = 2708 keV) of ^{86}Zr(2) due to its poor statistics. In addition, the lowest (E_γ = 1866 keV) and highest (E_γ = 2429 keV) transitions of ^{86}Zr(3) have been ignored in the fit for the same reason. We have chosen to ignore the tentative transitions because smaller rms deviation and a better agreement with experimental band head spin is obtained.

An illustrative example of least-squares fitting of ^{86}Zr(1) is given in Table 2. It is clear from the table that at I_0 = 24, rms deviation is at a minimum. However, if I_0 is assumed to be 23 or 25, rms deviation increases immensely, so both of these values have been discarded. The values of parameters $\Im_0$ and C obtained from a least-squares fit using the VMI model are listed in Table 3 and the softness parameter (σ) is derived from them. The experimental and calculated transition energies along with moment of inertia ($\Im_I$) of four SD bands in ^{86}Zr are shown in Table 4. Since at low spins the transition energy of ^{86}Zr(4) lies in the midpoint of ^{86}Zr(2), it was proposed [26] that these two could be signature partners. Hence, the spins of ^{86}Zr(4) should be 1$\hbar$ higher than those of ^{86}Zr(2). Also, it was measured [26] that the transition quadrupole moments (Q_t) of ^{86}Zr(4) ($=3.8^{+0.6}_{-0.5}$ eb) are close to ^{86}Zr(2), which further supports that these bands are signature partners. The calculated band head spin of ^{86}Zr(4) is 1$\hbar$ higher than ^{86}Zr(2) and the band head MOI of these two bands are very close to each other, which also supports the conjecture that these two are signature partner bands.

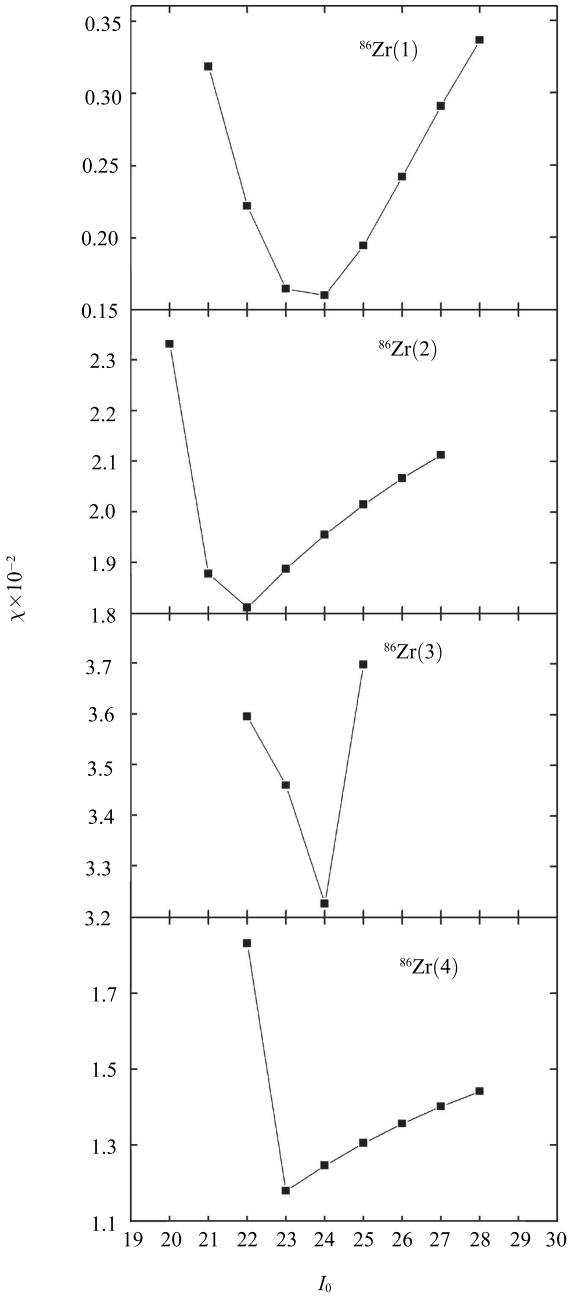

Fig. 1. χ plots to obtain band head spin (I_0) using the VMI model.

Table 2. Spin determination of ^{86}Zr(1) using the VMI model. I_0 corresponds to band head spin. $\delta = E_\gamma^{\rm exp}(I) - E_\gamma^{\rm cal}(I)$, where E_γ is in keV. χ is the rms deviation given by Eq. (21).

$E_\gamma^{\rm exp}(I)$	$I_0 = 23$[i]			$I_0 = 24$[ii]			$I_0 = 25$[iii]		
	I	$E_\gamma^{\rm cal}(I)$	δ	I	$E_\gamma^{\rm cal}(I)$	δ	I	$E_\gamma^{\rm cal}(I)$	δ
1518	25	1512.98	5.020	26	1516.09	1.905	27	1518.8	−0.8
1646	27	1649.23	−3.226	28	1650.36	−4.362	29	1651.33	−5.328
1785	29	1788.47	−3.470	30	1788.11	−3.107	31	1787.76	−2.761
1929	31	1930.94	−1.937	32	1929.58	−0.581	33	1928.37	0.626
2077	33	2076.85	0.146	34	2075.04	1.961	35	2073.44	3.561
2228	35	2226.45	1.554	36	2224.73	3.268	37	2223.23	4.767
2383	37	2379.94	3.059	38	2378.91	4.085	39	2378.03	4.971
2540	49	2537.56	2.437	40	2537.84	2.161	41	2538.1	1.899
2696	41	2699.54	−3.540	42	2701.76	−5.757	43	2703.72	−7.722
χ		0.00164488			0.00159806			0.00194048	

[i] $\Im_0 = 0.0339$ keV^{-1}, $C = 1.598\times10^8$ keV^3. [ii] $\Im_0 = 0.0357$ keV^{-1}, $C = 1.169\times10^8$ keV^3. [iii] $\Im_0 = 0.0375$ keV^{-1}, $C = 0.883\times10^8$ keV^3.

Table 3. Parameters obtained from least-squares fit of four bands in ^{86}Zr using the VMI model. The softness parameter (σ) is obtained using Eq. (8).

SD band	experimental $E_\gamma(I_0+2\rightarrow I_0)$/keV	band head MoI $\Im_0$/keV^{-1}	stiffness constant $(C\times10^8)$/keV^3	softness parameter $\sigma = 1/(2C(\Im_0)^3)$ $(\times10^{-5})$	χ $(\times10^{-2})$
^{86}Zr(1)	1518	0.0357	1.169	9.40	0.1598
^{86}Zr(2)	1577	0.0296	6.991	2.77	1.811
^{86}Zr(3)	1866	0.0301	7.153	2.56	3.22
^{86}Zr(4)	1648	0.0294	13.354	1.47	1.179

Table 4. Experimental transition energies ($E_\gamma^{\rm exp}$), calculated transition energies ($E_\gamma^{\rm cal}$) and moment of inertia ($\Im_I$) for SD bands in ^{86}Zr. For each band of ^{86}Zr, the first row corresponds to spin values, the second and third rows give experimental and calculated transition energies respectively, and the fourth row gives the moment of inertia obtained from the VMI model. Here E_γ is given in keV and $\Im_I$ in $\hbar^2$keV^{-1}. E_γ values marked by asterisks ($*$) represent tentative transitions.

^{86}Zr(1)									
I	26	28	30	32	34	36	38	40	42
$E_\gamma^{\rm exp}$	1518	1646	1785	1929	2077	2228	2383	2540	2696
$E_\gamma^{\rm cal}$	1516.09	1650.36	1788.11	1929.58	2075.04	2224.73	2378.91	2537.84	2701.76
$\Im_I$	0.0362	0.0365	0.0369	0.0373	0.0376	0.0380	0.0384	0.0388	0.0392
^{86}Zr(2)									
I	24	26	28	30	32	34	36	38	40
$E_\gamma^{\rm exp}$	1577	1730	1891	2056	2227	2393	2514	2562	2708*
$E_\gamma^{\rm cal}$	1613.84	1755.87	1899.04	2043.44	2189.17	2336.32	2484.97	2365.21	2787.14
$\Im_I$	0.0297	0.0298	0.02985	0.0299	0.0300	0.03014	0.03025	0.03036	0.03048
^{86}Zr(3)									
I	26	28	30	32	34	36	38		
$E_\gamma^{\rm exp}$	1866*	1959	2062	2155	2244	2343	2429*		
$E_\gamma^{\rm cal}$	1721.79	1861.79	2002.9	2145.23	2288.83	2433.81	2580.23		
$\Im_I$	0.030229	0.030312	0.030399	0.030493	0.030591	0.030693	0.030799		
^{86}Zr(4)									
I	25	27	29	31	33	35	37		
$E_\gamma^{\rm exp}$	1648	1811	1967	2123	2273	2403	2491		
$E_\gamma^{\rm cal}$	1679.89	1819.72	1960.14	2101.34	2243.22	2385.88	2529.37		
$\Im_I$	0.0295	0.02953	0.0296	0.02963	0.0297	0.02975	0.02981		

Parameters a,b and A,B,C of the ab formula and Harris ω^2 expansion respectively are used to calculate the dynamic moment of inertia. The dynamic MOI from the VMI model is calculated using Eq. (20). The variation of $\Im^{(2)}$ with $\hbar\omega$ is shown in Fig. 2. In the figure experimental data is shown by squares with error bars and calculated results are shown by triangles, stars and circles for the VMI model, ab formula and Harris ω^2 expansion respectively. The ab formula does not produce any general trend of $\Im^{(2)}$ and shows a constant variation with rotational frequency. Gradual downsloping behaviour of $\Im^{(2)}$ with $\hbar\omega$ was observed by Sarantittes et al. [26] in ^{86}Zr(1), which was interpreted as a loss of collectivity and increase in triaxiality of band. This trend of ^{86}Zr(1) is reproduced very well with the VMI model and Harris ω^2 expansion. The general trend of $\Im^{(2)}$ with $\hbar\omega$ for ^{86}Zr(2) and ^{86}Zr(4) is also reproduced well with Harris ω^2 expansion, although the VMI model does not reproduce the sudden increase of $\Im^{(2)}$ at higher frequency in ^{86}Zr(4). The high value of $\Im^{(2)}$ in ^{86}Zr(3) is intriguing, since the calculations done by Sarantittes et al. for both triaxial superderformed bands and enhanced deformation bands do not agree with experimental data. These high values of $\Im^{(2)}$ are reproduced well with Harris ω^2 expansion, but comparatively low values of $\Im^{(2)}$ are obtained from the VMI model.

The rigidity of the nucleus is defined by the nuclear softness parameter (σ) which increases as the deformation increases. The observed nuclear softness parameter for SD bands [39] is in the range $10^{-4} \leqslant \sigma \leqslant 10^{-6}$ due to their rigid rotor behaviour, whereas for ND bands [34] the range is $10^{-2} \leqslant \sigma \leqslant 10^{-4}$. As expected, our result for the softness parameter ($\sigma \sim 10^{-5}$) lies in the SD range.

4 Conclusion

The band head spin of four bands in ^{86}Zr has been proposed by the VMI model, ab formula and Harris ω^2 expansion. Out of the three rotational energy formulae, the band head spin obtained from the VMI model agrees with the available experimental results. Assigned spins for the lowest levels are $24\hbar$, $22\hbar$, $24\hbar$ and $23\hbar$ for ^{86}Zr(1), ^{86}Zr(2), ^{86}Zr(3) and ^{86}Zr(4) respectively. Whenever accurate band head spin is assigned, the calculated transition energies agree well with the experimental transition energies. The variation of $\Im^{(2)}$ with $\hbar\omega$ was also investigated. It can be concluded that the VMI model is a powerful approach in assigning spin not only of axially symmetric SD bands but also of triaxial SD bands. It was futher observed that Harris ω^2 expansion is a powerful tool for reproducing the experimental trend of $\Im^{(2)}$ with $\hbar\omega$.

Financial support from the Department of Science and Technology, Government of India is gratefully acknowledged.

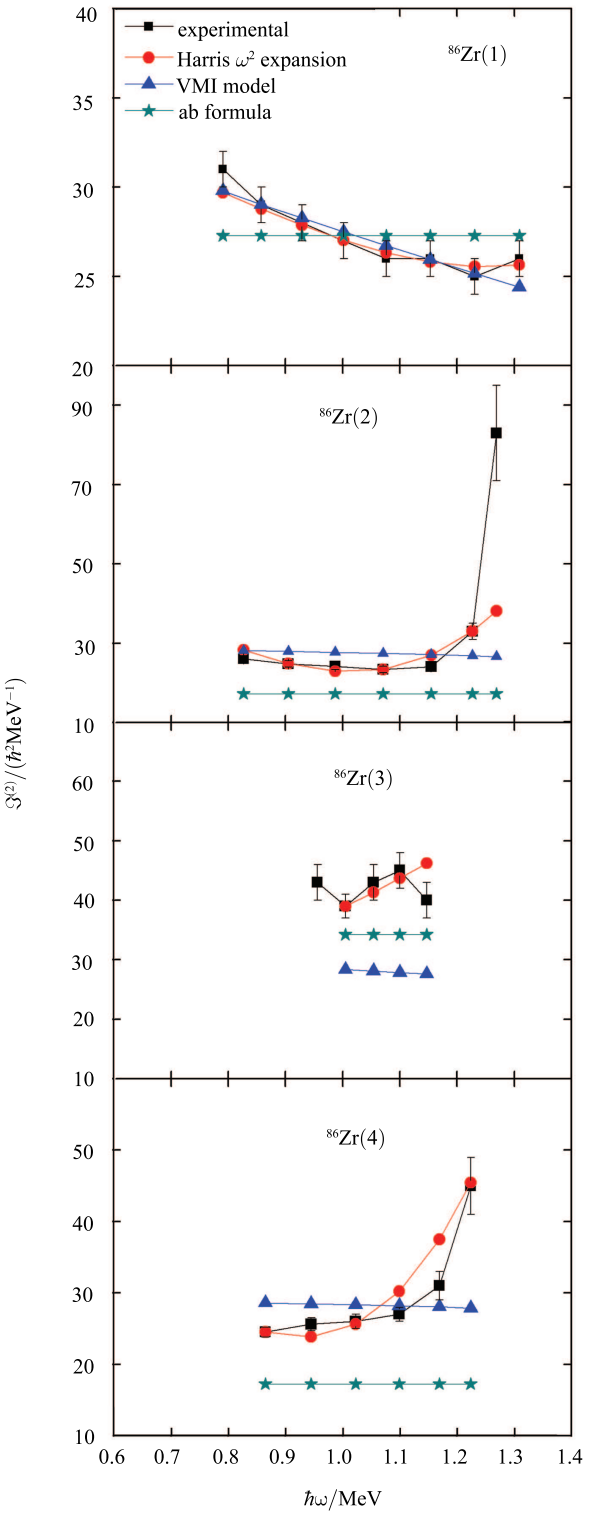

Fig. 2. Variation of calculated dynamic moment of inertia with rotation frequency for ^{86}Zr and comparison with experimental data. Experimental data is taken from Ref. [36]

References

1 V. M. Strutinsky, Nucl. Phys. A, **122**: 1 (1968)
2 P. J. Twin et al, Phys. Rev. Lett., **57**: 811 (1986)
3 T. L. Khoo et al, Phys. Rev. Lett., **76**: 1583 (1996)
4 K. Hauschild et al, Phys. Rev. C, **55**: 2819 (1997)
5 A. Lopez-Martin et al, Phys. Lett. B, **380**: 18 (1996)
6 M. J. Brinkman et al, Phys. Rev. C, **53**: R1461 (1996)
7 G. Hackman et al, Phys. Rev. Lett., **79**: 4100 (1997)
8 J. A. Becker et al, Phys. Rev. C, **46**: 889 (1992)
9 J. Y. Zeng et al, Phys. Rev. C, **44**: R1745 (1991)
10 R. Piepenbring and K. V. Protasov, Z. Phys. A, **345**: 7 (1993)
11 F. R. Xu and J. M. Hu, Phys. Rev. C, **49**: 1449 (1994)
12 S. G. Zhou and C. Zheng, Phys. Rev. C, **55**: 2324 (1997)
13 Z. H. Zhang et al, Phys. Rev. C, **87**: 054308 (2013)
14 S. G. Zhou et al, Nucl. Phys. A, **615**: 229 (1997)
15 M. A. Riley et al, Nucl. Phys. A, **512**: 178 (1990)
16 M. W. Drigert et al, Nucl. Phys. A, **530**: 452 (1991)
17 Y. Sun et al, Phys. Rev. Lett., **78**: 2321 (1997)
18 Y. Liang et al, Phys. Rev. C, **46**: R2136 (1992)
19 Y. Sun et al, Phys. Rev. Lett., **83**: 686 (1999)
20 Y. Sun et al, Phys. Rev. C, **52**: R2844 (1995)
21 C. Baktash et al, Phys. Rev. Lett., **74**: 1946 (1995)
22 W. Schmitz et al, Phys. Lett. B, **303**: 230 (1993)
23 H. Schnack-Petersen et al, Nucl. Phys. A, **594**: 175 (1995)
24 C. X. Yang et al, Eur. Phys. J. A, **1**: 237 (1998)
25 J. C. Bacelar et al, Nucl. Phys. A, **442**: 547 (1995)
26 D. G. Sarantites et al, Phys. Rev. C, **57**: R1 (1998)
27 A. Bohr and B. R. Mottelson, *Nuclear Structure* (Benjamin, New York, 1975), Vol. 2, Chap. 4
28 S. M. Harris, Phys. Rev. Lett., **13**: 663 (1964)
29 S. M. Harris, Phys. Rev., **138**: A509 (1965)
30 P. Holmberg and P. O. Lipas, Nucl. Phys. A, **117**: 552 (1968)
31 C. S. Wu and J. Y. Zeng, Commun. Theor. Phys. (Beijing), **8**: 51 (1987)
32 C. S. Wu et al, Phys. Rev. C, **45**: 261 (1992)
33 C. S. Wu et al, Phys. Rev. C, **45**: 2507 (1992)
34 M. A. J. Marriscotti, G. S. Goldhaber and B. Buck, Phys. Rev., **178**: 1864 (1969)
35 S. X. Liu and J. Y. Zeng, Phys. Rev. C, **58**: 3266 (1998)
36 X. L. Han and C. L. Wu, At. Data Nucl. Data Tables, **73**: 43 (1999)
37 B. Singh, R. Zywina and R. B. Firestone, Nucl. Data Sheets, **97**: 241 (2002)
38 http://www.nndc.bnl.gov/
39 N. Sharma, H. M. Mittal, S. Kumar and A. K. Jain, Phys. Rev. C, **87**: 024322 (2013)